Conceptual Design of Boundary Layer Ingesting Aircraft Capturing Aero-Propulsive Coupling

Jai Ahuja* and Dimitri N. Mavris †
Aerospace Systems Design Laboratory, School of Aerospace Engineering,
Georgia Institute of Technology, Atlanta, GA, 30332, USA

The impacts of boundary layer ingestion on aircraft performance can be modeled using either a decoupled or a coupled approach. Several studies in literature have adopted the former, while some have shown differences between the two approaches for the performance analysis and design refinement of a sized aircraft. This study quantifies the consequences of ignoring aero-propulsive coupling at the aircraft sizing stage of conceptual design. To do so, a parametric and coupled aero-propulsive design methodology is used that leverages surrogate modeling to minimize the expense of computational fluid dynamics in generating estimates of the boundary layer ingestion performance impacts. The method is applied to the design and analysis of two aircraft in the 150 passenger class, with different engine locations. Discrepancies in block fuel burn estimates, as large as 2.15%, were found to occur by ignoring aero-propulsive interactions.

I. Nomenclature

A_{PI}	=	area of propulsor inlet integration plane
A_{PO}	=	area of propulsor outlet integration plane
D'	=	non-BLI aircraft drag
d_2	=	fan diameter
F'_N	=	gross thrust minus freestream ram drag
h	=	altitude
M	=	Mach number
P_{ex}	=	excess power required
$P_{K_{\text{in}}}$	=	ingested mechanical energy defect ($C_{P_{K_{\text{in}}}}$ is the non dimensional form)
p	=	static pressure
p_t	=	total pressure

*Postdoctoral Fellow
†S.P. Langley Distinguished Regents Professor, AIAA Fellow
Presented as Paper 2021-0112 at the AIAA SciTech 2021 Forum, Virtual Event, January 11–15 and 19–21, 2021

S	=	wing planform area
S_{ref}	=	reference area
SPW_{c_2}	=	specific corrected flow at fan face
V	=	flow velocity magnitude vector
$\mathbf{V}$	=	flow velocity vector
$\mathbf{x}$	=	vector of design variables
$\mathbf{x}_{\text{S}}$	=	vector of shared variables
$\mathbf{y}$	=	vector of coupling variables
$\mathbf{y}^t$	=	vector of target variables
Greek	=	
α	=	angle of attack
β	=	symbol representing BLI effects
Δ	=	change in the value of a given quantity
η_{PR}	=	pressure recovery
λ	=	taper ratio
$\Lambda_{c/4}$	=	quarter chord sweep angle
Λ_{LE}	=	leading edge sweep angle
ρ	=	density
ϕ	=	fuselage ramp angle (of the S-shaped inlet) feeding into the propulsor
Φ_{surf}	=	dissipation in aircraft surface boundary layer
Φ_{wake}	=	dissipation in aircraft wake
Conventions	=	
$(\cdot)'$	=	non-BLI quantities
$(\cdot)_{\text{A}}$	=	quantities related to the aerodynamics discipline
$(\cdot)_{\text{B}}$	=	quantities related to the BLI effects model
$(\cdot)_{\text{P}}$	=	quantities related to the propulsion discipline
$(\cdot)_\infty$	=	freestream quantities

II. Introduction

Given the impact of fuel prices on airline operating costs, it should be no surprise that reduced fuel burn is one of the primary design drivers for each new generation of aircraft. Reductions in block fuel burn, even as small as 0.25%, can have a substantial fleet level impact. Entities like National Aeronautics and Space Administration in the United

States, and the Advisory Council for Aeronautics Research in Europe, are spearheading research efforts into concepts and technologies for improved fuel efficiency [1, 2]. One promising set of concepts are Boundary Layer Ingesting (BLI) aircraft. As shown by Betz [3], the low velocity inflow for BLI propulsors reduces the power required to produce a given net momentum flux, which directly translates to fuel burn savings. There are several entities all over the world actively involved in investigating BLI applications for a range of aircraft passenger classes, including regional jets [4], single aisle class concepts such as the STARC-ABL [5], D8 Double Bubble [6–8], and the Onera NOVA-BLI [9], as well as larger vehicles such as a BLI variant of the Common Research Model [10] and the N3-X Turboelectric Distributed Propulsion (TeDP) Blended Wing Body (BWB) [11, 12] to name a few.

Concepts like these exhibit stronger interactions between the airframe aerodynamics and propulsion system, relative to conventional designs with podded engines, owing to the propulsor-airframe integration. The flow ingested by the propulsor, and the corresponding propulsor performance, is strongly dependent on the airframe aerodynamics, which in turn is affected by the propulsor design and operation. As such, any initial assumptions made by one disciplinary analysis regarding the other, must be updated based on the outputs from the latter in an iterative manner till there is consistency between the two disciplines. Thus, aerodynamics and propulsion are "coupled" for BLI vehicles and cannot be considered in isolation. Several studies, such as those by Rodriguez [13], Gray [14–17], Kim [18, 19], Felder [12], and Bijewitz [20] for example, have accounted for these aero-propulsive interactions to varying extents.

However, a significant number of BLI studies decouple the airframe and propulsion system design and/or analysis. In other words, the aero-propulsive interactions are ignored and there is no iterative exchange of information between disciplines. Examples include conceptual proposals for the BWB variants [21–27], D8, STARC-ABL, NOVA-BLI, and early studies on the propulsive fuselage concept [28]. Decoupled approaches are particularly amenable in early conceptual design since, as Hendricks [29] notes, these approaches do not need an integrated design environment which coordinates the execution of and the exchange of information between the aerodynamics and propulsion analysis codes. This enables a "traditional division of modeling"[29], allowing researchers to focus on their areas of expertise and use any fidelity level for modeling their disciplines, without having to incur the computational expense of ensuring compatibility with other disciplinary tools. Rapid design space exploration is thus possible early on.

Decoupled approaches however fail to capture the interdependency between aerodynamics and propulsion, and the results are inconsistent between the two disciplines. Felder's work with the N3X engine [12] for example showed differences in propulsive efficiency between coupled and decoupled approaches. Gray's analysis of the STARC-ABL [14, 16] showed differences in fan face total pressure and boundary layer profiles as a result of aero-propulsive interactions. The vehicle sized using a decoupled approach is dependent on the validity of the assumptions used for modeling the BLI impact, imparting an additional degree of uncertainty in the performance of the proposed concept. Additionally, maximizing fuel burn benefits for BLI concepts requires propulsion-airframe integration efforts that maximize favorable and minimize detrimental interactions between the airframe and propulsor. Decoupled approaches

cannot be used to optimize the integrated vehicle since they do not capture this interaction.

The objective of this paper is to quantify the consequences of ignoring the aero-propulsive coupling resulting from BLI in the initial stages of conceptual design. For a specified mission and constraints, a coupled design approach is compared to a decoupled approach, looking at differences in design parameters such as wing planform area and fan diameter, and performance metrics like block fuel burn and takeoff gross weight (TOGW). This effort entails i) defining and isolating the impacts of BLI on vehicle performance ("BLI effects") ii) developing correlations that map changes in airframe and propulsor design/operation to the BLI effects and iii) integrating these expressions in a vehicle sizing environment. The BLI coupled and decoupled methodologies are implemented in the Environmental Design Space (EDS) framework [30, 31]. EDS integrates the aircraft mission analysis code FLOPS [32], engine cycle analysis code NPSS [33], engine weights and flowpath estimation code WATE++ [34], and other analysis modules for overall vehicle sizing and performance assessment.

Section III provides an overview of the BLI effects modeling approach, with details on the CFD models in section IV. Section V describes the differences between the decoupled design methodology and the proposed coupled approach, and sections VI and VII describe the design and analysis process for two 150 passenger class BLI concepts, highlighting differences in design and performance characteristics due to aero-propulsive coupling. Finally, section VIII summarizes key takeaways from this study.

III. BLI Performance Impacts (BLI Effects)

To capture the aero-propulsive interactions due to BLI, one must first define a way to model the BLI performance impacts. The idea here is to treat BLI like a technology and define an appropriate set of responses that can be applied to a non-BLI configuration to determine how this design will perform when BLI is now considered. Changes to airframe and propulsor design variables for conventional aircraft with podded engines are captured through changes in drag and thrust respectively. However, this decomposition is ambiguous for BLI concepts. Drela's power balance approach [35] is one solution. This formulation bookkeeps performance as power sources and power sinks, instead of the ill-defined thrust and drag. However, most existing engine and airframe codes still rely on thrust-drag, so a mapping between power balance and thrust-drag is needed that is unambiguous and correctly captures the BLI related physics. It is important to recognize that the power balance formulation is valid for both BLI and non-BLI configurations. Therefore, power balance must also be equivalent in some manner to thrust-drag bookkeeping for non-BLI aircraft. From the first observation, it is possible to relate the power balance equation for a BLI aircraft to the non-BLI formulation and identify major changes in dissipation that occur as a result of the engines ingesting the boundary layer. These terms that capture the changes in the propulsive power requirements due to boundary layer ingestion can be called the BLI effects. The second observation then allows one to formulate a thrust-drag bookkeeping scheme for BLI aircraft that accounts for the impacts of BLI using the power balance terminology, as shown below:

$$F'_N V_\infty = D' V_\infty + P_{\text{ex}} - \underbrace{\left(P_{K_{\text{in}}} + \Delta\Phi_{\text{wake}} + \Delta\Phi_{\text{surf}}\right)}_{\beta} \tag{1}$$

The derivation of Eq. (1) was based on the work by Hall [36, 37] and Drela [35]. Details of this derivation can be found in a previous paper by the authors [38]. In Eq. (1), F'_N is the gross thrust minus the freestream ram drag, D' is the drag of the un-powered airframe, P_{ex} represents the excess power requirement, and β represents the BLI effects. Thus, Eq. (1) basically states that the power produced by the propulsor must balance the power required by the aircraft, the excess power requirements, and any propulsive power changes due to BLI. A general description of the relevant BLI effects and comments on the implementation strategy for this study are presented below.

A. Description of BLI Effects

1. $P_{K_{in}}$

This term captures the ingested mechanical energy defect rate by the propulsor and is one of the major contributors to a reduction in propulsive power. This quantity is defined by the following equation:

$$P_{K_{\text{in}}} = \iint -\left[(p - p_\infty) + \frac{1}{2}\rho\left(V^2 - V_\infty^2\right)\right]\mathbf{V}\cdot\hat{\mathbf{n}}\,dA_{PI} \tag{2}$$

This surface integral can be evaluated on a disc at the inlet highlight plane (as done by Hall [37]), or at the fan-face, for a powered engine. The highlight plane ignores contributions from the inlet, which is justifiable for early conceptual design since the inlet geometry is still ill-defined. However, [39] shows a non-negligible contribution from the inlet to $P_{K_{\text{in}}}$, which is why the fan-face annulus is chosen as the integration plane in this study.

2. $\Delta\Phi_{wake}$

Captures the change in power dissipation in the airframe wake due to partial wake ingestion by the propulsor. The method suggested in [37] approximates this change as the reduction in amount of mechanical flow energy being deposited off the airframe, calculated using the equation below, evaluated at the propulsor outlet plane

$$\Delta\Phi_{\text{wake}} \approx \iint \left[\frac{1}{2}\rho|\mathbf{V} - \mathbf{V}_\infty|^2\mathbf{V}\cdot\hat{\mathbf{n}} + (p - p_\infty)\,(\mathbf{V} - \mathbf{V}_\infty)\cdot\hat{\mathbf{n}}\right] dA_{PO} \tag{3}$$

It is important to highlight that $\Delta\Phi_{\text{wake}}$ is estimated from an un-powered configuration. Integrating Eq. (3) at the propulsor outlet plane (A_{PO}) to calculate $\Delta\Phi_{\text{wake}}$ has the following reasoning: by placing a propulsor at that location, these perturbations in the flow are ingested and thus will not dissipate in the airframe wake. With a powered engine jet, this reasoning is not valid given that perturbations in the flow arise primarily from the jet, and not from the ingested wake. Thus, an un-powered configuration needs to be defined to calculate $\Delta\Phi_{\text{wake}}$.

This un-powered configuration is the same as the BLI airframe, with two possible ways for dealing with the engine. The first way, as done by Hall, uses a through-flow nacelle. An integration area is defined at the nozzle exit plane on which Eq. (3) is calculated. The alternative is to eliminate the through-flow nacelle geometry altogether and just leave the appropriately sized integration plane on which $\Delta\Phi_{\text{wake}}$ can be evaluated. The change fan/nacelle diameter and the corresponding change in the amount of BLI can be captured quite easily by varying the radius of the integration area within a CFD run, without having to run additional cases. For simplicity, this change in integration plane radius can be set equal to the change in fan radius. While the impact of the nacelle geometry on the upstream flow is not captured in this approach, it is expected that $\Delta\Phi_{\text{wake}}$ is much more sensitive to the amount of boundary layer ingested for these un-powered cases. As such, reasonable estimates for $\Delta\Phi_{\text{wake}}$ can be obtained from this pragmatic approach.

3. $\Delta\Phi_{surf}$

Captures the change in power dissipation in the boundary layer over the airframe surface. The change in surface dissipation can be modeled by the change in wetted area going from the podded to the BLI configuration. Elimination of the pylons and partial embedding of the engines in the airframe, for example, contribute to reductions in wetted area. The following sub-section explains how geometry changes are mapped to wetted areas for a parametric model.

4. η_{PR}

Though not an explicit part of Eq. (1), pressure recovery affects the fuel flow required by the propulsor to produce a given F'_N. Pressure recovery and $P_{K_{\text{in}}}$ must be calculated at the same location. Otherwise, there is an inconsistency in bookkeeping losses and performance benefits. If $P_{K_{\text{in}}}$ is evaluated at the inlet highlight (station 1), pressure recovery is defined as p_{t_1}/p_{t_∞} and thus only captures total pressure losses in the boundary layer over the airframe surface. If inlet contributions are to be accounted for, as done in this study, $\eta_{PR} = p_{t_2}/p_{t_\infty}$, where station 2 is the fan face.

B. Parametric Models of the BLI Effects

Single operating point aero-propulsion design analyses or optimization studies can be conducted by directly linking CFD to an engine cycle analysis code, leveraging state of the art gradient based optimization techniques, as done in several works cited above. For BLI aircraft sizing, such approaches are not practical given the sheer number of function calls that would be required and the associated computational cost. For sizing and mission analysis, there is a need to capture the BLI impacts on performance for every perturbation in airframe and engine design variables, as well as flight conditions for every point in the mission. As such, one way to alleviate the computational burden of using CFD to model the BLI effects is through the use of surrogate modeling techniques. These models provide functional relationships between the BLI effects and changes in key parameters of interest. These semi-empirical performance corrections can then be integrated within a conceptual design framework for coupled aero-propulsion BLI vehicle sizing.

1. Design Space Parameterization

Based on the studies presented in [38] and [39], key airframe and propulsor variables affecting the BLI effects were identified. From that, a smaller subset of variables is picked for the BLI surrogates, summarized in Table 1. Bounds on the wing design variables represent a realistic design space for a 150-180 pax aircraft. Limits on the Mach-altitude (M_∞-h) operating zone and specific corrected flow (SPW_{c_2}) are shown in Fig. 1. The former envelope is based on engineering judgment and existing aircraft operations, while the latter represents physical limitations of the non-BLI engine at different flight conditions. Black lines show the constrained operating envelope for the BLI surrogates. Boundary layer blockage effects limit the maximum specific corrected flow value. Higher values result in a choked inlet. Constraints imposed on the operating space avoid wastage of computational resources by sampling in regions that are unlikely to be encountered in a typical mission.

Table 1 BLI Surrogate Model Input Variables

Input Variable	Lower Bound	Upper Bound	Type	Associated BLI Effects
S (ft^2)	1076	1722	Airframe	$P_{K_{\text{in}}}$ and η_{PR}
Aspect Ratio (AR)	7	11	Airframe	$P_{K_{\text{in}}}$ and η_{PR}
Λ_{LE} (°)	20	40	Airframe	$P_{K_{\text{in}}}$ and η_{PR}
λ	0.2	0.4	Airframe	$P_{K_{\text{in}}}$ and η_{PR}
ϕ (°) (see Fig. 2)	12	20	Airframe	All
d_2 (in)	68	78	Propulsor	All
SPW_{c_2} (lbm/ft^2-s)	$f(M_\infty)$	44	Propulsor	$P_{K_{\text{in}}}$ and η_{PR}
M_∞	0.25	0.85	Flight conditions	$P_{K_{\text{in}}}$ η_{PR} $\Delta\Phi_{\text{wake}}$
h (ft)	0	43000	Flight conditions	$P_{K_{\text{in}}}$ η_{PR} $\Delta\Phi_{\text{wake}}$
α (°)	0	4	Flight conditions	$P_{K_{\text{in}}}$ η_{PR} $\Delta\Phi_{\text{wake}}$

The irregular nature of the BLI surrogate input space stemming from constraints on the M_∞-h-SPW_{c_2} envelope warrants a computer generated custom design of experiments (DOE). In the statistical software, JMP, an I-optimal space-filling DOE is created, which minimizes the prediction variance over the entire design space, thereby improving the precision of the predictions made by the surrogate models [40]. Each row in the DOE represents a unique combination of geometry and operating conditions. A geometry model and CFD simulation need to be created for each case.

2. Preparing Geometry Models for CFD Analysis of BLI Effects

OpenVSP [42], a parametric aircraft geometry generation tool, is used to create baseline templates for the two BLI configurations considered in this study, shown in Fig. 2. The only differences between these two variants are the engine location and tailcone design. The length of the fuselage, at 128 ft, is based off a notional 737-8. The fuselage width, at 17.6 ft, was driven by the need to fit two BLI engines on top of the fuselage. Both templates also share the same wing design, which is a scaled version of the Common Research Model [43] wing. No empennage is included in the templates

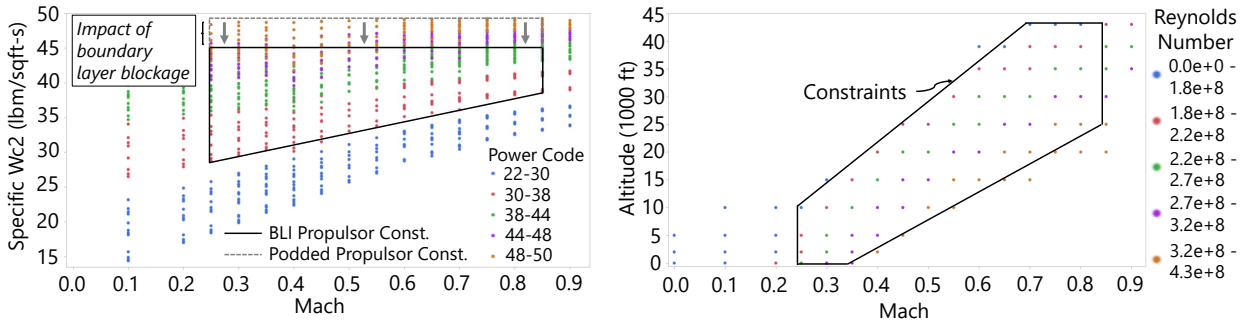

(a) M_∞-SPW_{c_2} (b) M_∞-h

Fig. 1 Operating envelopes for the BLI aircraft (adapted from [41])

since the impact of the tails is mostly on the fuselage trailing edge mounted propulsor, which is not considered in this study. However, the y location of the engine and the maximum diameter are constrained for the top mounted engine configuration to integrate a vertical tail on the sides, like on the D8 concept.

The nacelle length, inlet length, highlight diameter, and fan diameter are extracted from outputs of a notional CFM LEAP-1B engine model, built in NPSS and WATE++, to create a simplified nacelle model in OpenVSP. The mechanical design, geometry, thermodynamic cycle, and performance characteristics of this notional engine model are developed and calibrated using sources such as European Union Aviation Safety Agency's ICAO aircraft engine emissions databank [44] and type-certificate data sheet [45]. Additional details regarding the general process for engine model calibration in EDS can be found in [31]. The architecture for this baseline engine model is shown in Fig. 2. Key cycle characteristics used in the NPSS model are presented in Table 2, quoted at Mach 0.8 at an altitude of 35,000 ft. Since WATE++ does not provide any information on the outer nacelle curvature and inlet throat diameter, as evident in Fig. 2, these detailed characteristics were approximated from literature on the STARC-ABL tailcone nacelle.

Perturbations to the geometry templates in OpenVSP are executed through a Python script. Only the geometry

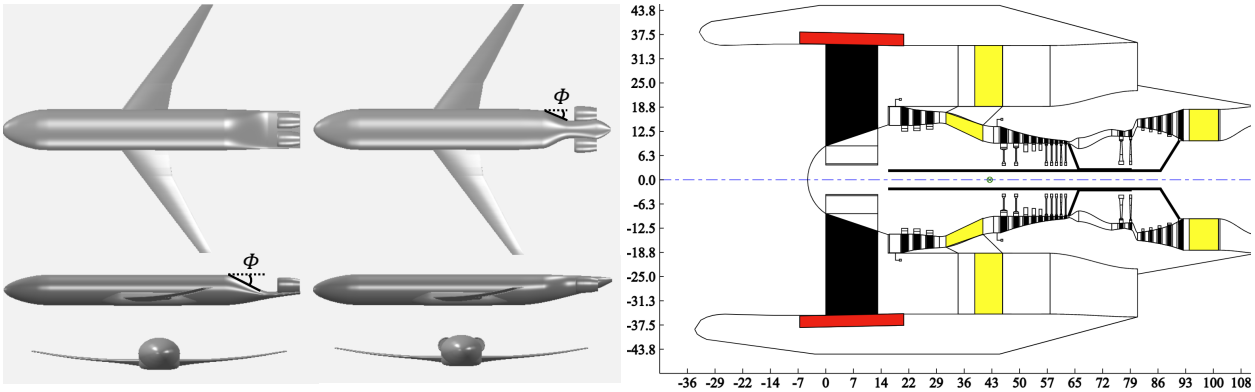

(a) 3-views of the baseline aircraft geometry templates (adapted from [41])

(b) Baseline engine architecture (dimensions in inches)

Fig. 2 Templates used for generating the geometry for each DOE case

Table 2 Baseline Engine Characteristics

Parameter	Value
Fan Pressure Ratio (FPR)	1.54
Bypass Ratio (BPR)	10.05
Low Pressure Compressor Pressure Ratio (LPCPR)	1.55
High Pressure Compressor Pressure Ratio (HPCPR)	20.25
Overall Pressure Ratio (OPR)	47.6
Fan Diameter (in)	70
Sea Level Static Thrust/Engine (lb)	29315

parameters in Table 1 are varied for each case in the DOE. All other geometry characteristics are fixed and no aerodynamic shape optimization is conducted for each run. Wing planform area and leading edge sweep are adjusted directly through the manipulation of OpenVSP's area and sweep variables. Aspect ratio perturbations involve an iterative process of adjusting the wing span and planform area variables to meet the specified targets. Varying the fuselage ramp angle feeding into the propulsor, ϕ, involves changing the width of the fuselage cross section just in front of the propulsor for the side-mounted engine case, and the height of the cross section for the top-mounted engine configuration. For the nacelle, only the fan tip and hub diameters are changed, keeping the same hub to tip ratio. The inlet and total nacelle length, and the contouring of the nacelle are unchanged. The highlight to throat, and highlight to fan annulus area ratios are also kept the same. Through the use of "Advanced Links" in OpenVSP, a design relation can be set up that automatically adjusts the nacelle position any time the fan diameter and/or the fuselage ramp angle are changed. This rule ensures that the nacelles remain partially embedded in the fuselage for each DOE case. For the CFD runs needed to compute $\Delta\Phi_{\text{wake}}$, the nacelle is excluded from the geometry model. A step file is created for each case in the DOE and is then imported into the CFD program.

3. Surrogate Modeling

Second order response surface models are developed for the BLI effects, using powered CFD results for $P_{K_{\text{in}}}$ and η_{PR}, un-powered CFD for $\Delta\Phi_{\text{wake}}$, and geometry information for $\Delta\Phi_{\text{surf}}$. The impacts of $\Delta\Phi_{\text{surf}}$ can be accounted through corrections to the wetted areas used by FLOPS for its parasitic drag predictions. Specifically, the FLOPS internally computed wetted areas for the nacelle and fuselage, which do not account for partially embedded nacelles, can be overwritten by user specified values for SWETF (fuselage wetted area factor) and SWETN (nacelle wetted area factor) respectively. Wetted and theoretical area calculations for each component can be obtained from OpenVSP. The unique combinations of fan diameter (d_2) and fuselage ramp angle in the training DOE for $P_{K_{\text{in}}}$ and η_{PR} are used for training the SWETF and SWETN surrogates. For this study, SWETF is specified as a dimensional quantity for fuselage wetted area. SWETN on the other hand is specified as a ratio of the wetted area to theoretical surface area of

the nacelle, and is thus a scalar multiplier. This quantity captures the reduction in surface area due to partial embedding of the nacelle in the fuselage. SWETN then corrects FLOPS's estimation of the nacelle wetted area, which is based on nacelle dimensions calculated by WATE++. In [41], the reader can find a discussion on the diagnostic measures used to evaluate the generated surrogate models. Metrics like R^2, average error as a fraction of the mean response, actual vs. predicted trends, residual vs. predicted trends, model fit error distribution, and model representation error distribution are considered. In addition, predicted trends from the models are compared to previously published work in [38, 39]. All together, these diagnostics show strong support for the validity of the developed BLI effects surrogate models.

IV. CFD Modeling Approach

A. Comments on Solver

The commercial code STAR-CCM+ is used for the CFD simulations. Steady state conditions and standard atmosphere properties are assumed for this study. The solver uses an implicit time integration scheme with second order upwind spatial discretization, with the AUSM+ FVS method and the Venkatakrishnan limiter for evaluating the inviscid fluxes. Fully turbulent conditions are assumed, and the SST k-ω turbulence model is chosen. A spherical freestream boundary with a radius approximately 30 times the fuselage length is defined, and x-z plane symmetry allows for half the domain to be modeled. A multi-grid initialization strategy along with automatic CFL control are employed to improve solver convergence. The stopping condition for the simulation is satisfied when the change in the non-dimensional form of $P_{K_{\text{in}}}$ ($C_{P_{K_{\text{in}}}} \equiv P_{K_{\text{in}}}/q_\infty V_\infty S_{\text{ref}}$, with $S_{\text{ref}} = 1$ for convenience) is less than 10^{-4} over 1000 iterations.

B. Propulsor Modeling in CFD

The engine is modeled in CFD with powered boundary conditions, similar to the propulsor models in [13, 14, 46]. The fan face is treated as a pressure outlet with a uniform static pressure and temperature imposed at this plane. The fan exit is modeled as a stagnation inlet with uniform total pressure and temperature conditions. For any combination of specific corrected flow, Mach number, and altitude in the DOE derived from Table 1, a required mass flow rate can be computed. This flow rate is then imposed as a target in the CFD solver. The fan face static conditions are updated in an iterative manner by the solver till the computed flow rate matches the specified target.

The engine core is not considered in the CFD domain, even though it is part of the NPSS engine model. In this study, the flow downstream of the fan is of no interest because metrics like fan exit mass flow, or net axial force for example are not being computed in CFD. It can be assumed that the BLI effects discussed in Sec III.A are primarily affected by the ingested flow, which in turn does not depend on the geometry and boundary conditions downstream of the fan face *in the CFD domain*. Thus, the core and plug geometries can be excluded from the CFD model of the propulsor, thereby eliminating the need to carefully design these components, while also reducing the mesh size and overall computational expense. The fan exit boundary conditions are thus also not critical for computing the BLI effects, but still need to

be set appropriately to ensure proper CFD solver convergence. Throttle impacts on the fan exit boundary conditions are ignored, but Mach and altitude effects are captured. Values of fan pressure ratio at 1.5 and a pressure recovery of 0.96 are assumed for every point in the operating envelope. The fan exit total pressure is then computed as a product of the freestream total pressure, assumed fan pressure ratio, and pressure recovery. The total temperature at the fan exit can then be computed using isentropic relations, for the assumed fan pressure ratio, and assuming no loss in total temperature between freestream and the fan face.

C. Comments on Meshing

An unstructured Cartesian mesh is used for all cases, with prism layers for near wall refinement to capture the boundary layer. The near wall spacing is calculated such that a wall y-plus of less than one is achieved over majority of the outer mold line. Additional refinement in the tailcone region of the fuselage is achieved through the specification of volumetric refinement zones that encompass both the fuselage ramp feeding into the propulsor and the nacelle.

A grid refinement study is conducted for a single top-mounted engine configuration to find an appropriate and common set of grid settings that balance accuracy and computational expense for all cases in the DOE. The airframe design parameters for this geometry are approximately set to the center point of the design space shown in Table 1. The nacelle geometry and engine boundary conditions are obtained from the baseline engine model shown in Fig. 2 and Table 2. The implicit assumption that the mesh settings found for the top-mounted engine configuration are also valid for the side engine case is not unreasonable, given the similarities between both designs. However, to account for the differences in the tailcone region and the propulsor location, the position and extent of the volumetric refinement zones are adjusted. The cell sizes in these zones, however, are kept the same for both configurations.

This mesh study is conducted at Mach 0.8 at 35,000 ft, for a two degree angle of attack; a typical cruise flight condition. The fan face static and fan exit total conditions are held constant across all grid levels. These boundary conditions are obtained from NPSS for an assumed cruise power setting. Mass flow targeting is disabled for the grid

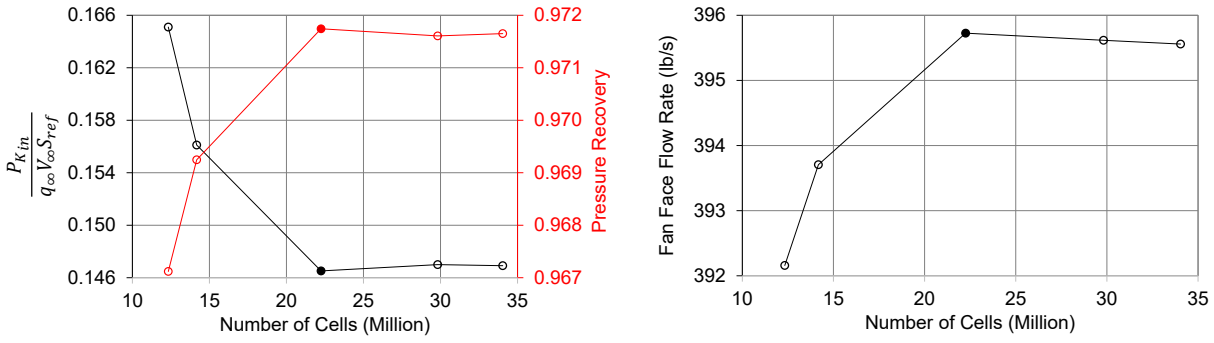

(a) $C_{P_{K_{\text{in}}}}$ and η_{PR} (b) $\dot{m}$

Fig. 3 Summary of results from mesh sensitivity trials (filled marker for final mesh) (adapted from [41])

refinement study. The results are shown in Fig. 3. The final mesh chosen is shown with a filled marker. The maximum variation in $C_{P_{K_{\text{in}}}}$ for finer meshes, relative to the chosen mesh, when dimensionalized to a force (recall S_{ref} is set to 1 for convenience), is approximately one pound at this flight condition. For pressure recovery and flow rate, the maximum difference between the chosen grid and finer grids is also quite small, at approximately 0.01% and 0.04% respectively.

V. Coupled and Decoupled BLI Aircraft Design Methodologies

This section describes the BLI coupled and decoupled aircraft sizing methodologies. Both approaches are similar except for how the BLI impacts on design and performance are considered. In the coupled approach, the impacts of BLI are updated in the iterative design process, while in the decoupled method, they are fixed at some initial estimate. Fig. 4 compares the coupled BLI sizing methodology to the decoupled approach as implemented in EDS.

A. Coupled BLI Aircraft Sizing

The BLI aircraft sizing loop begins with a specification of airframe parameters, ($\mathbf{x}_{\text{A}}$), engine parameters, ($\mathbf{x}_{\text{P}}$), and parameters shared by the engine, airframe, and BLI effects models ($\mathbf{x}_{\text{S}}$). These values are fixed for the sizing process, but can be changed as part of an outer loop design space exploration or optimization exercise. Initial guesses for the coupling variables related to each discipline ($\mathbf{y}^{t,(0)}$) are also specified. These parameters are used as inputs for NPSS, FLOPS, WATE++, the BLI surrogates, and other disciplinary analysis tools in EDS. Table 3 highlights what kind of variables each of the above vectors represent. Note that the list of airframe and propulsor design variables shown in Table 3 is not exhaustive. The shared and coupling variable lists, however, are complete. Process 1 in Fig. 4a is the engine design loop, which involves a feedback between engine sizing and the evaluation of BLI effects. The engine is sized using a multi-design point approach [47, 48] for a given set of propulsor variables and target values for the airframe coupling variables ($\mathbf{y}^t_{\text{A}}$). For this study, the selected engine design points are: 1) Aerodynamic Design Point (ADP), where the design turbomachinery cycle parameters are specified 2) Top of Climb (TOC), a critical sizing point for the fan as it sets the maximum mass flow and corrected speed 3) Takeoff (TKO), where the maximum temperature

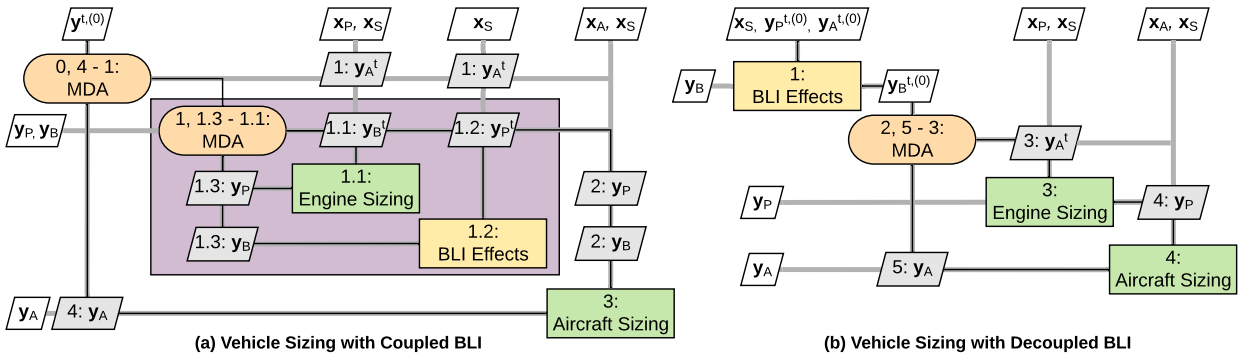

Fig. 4 Coupled and decoupled BLI effects accounting approaches for aircraft design (adapted from [41])

Table 3 Examples of Design Parameters and Coupling Variables

Parameter	Examples
$\mathbf{x}_{\mathrm{A}}$	Empennage volume coefficients, empennage: AR, λ, $\Lambda_{c/4}$, wing dihedral, component weight estimations: avionics, APUs, etc., component lengths, wing loading, thrust to weight ratio, etc.
$\mathbf{x}_{\mathrm{P}}$	Fan pressure ratio, bypass ratio, high and low pressure compressor pressure ratios, maximum fan specific flow, compressor and turbine hub to tip ratios, component efficiencies, assumed turbomachinery design characteristics like number of blades, aspect ratio, etc. for weight calculations, assumed duct losses, maximum turbine inlet temperature, etc.
$\mathbf{x}_{\mathrm{S}}$	Wing: AR, Λ_{LE}, λ, ramp angle ϕ, flight conditions
$\mathbf{y}_{\mathrm{A}}$	Wing planform area and thrust scaling factor (or thrust requirements at engine design points)
$\mathbf{y}_{\mathrm{P}}$	Fan diameter, max nacelle diameter, engine length, engine weight, engine deck
$\mathbf{y}_{\mathrm{B}}$	$P_{K_{\mathrm{in}}}$, η_{PR}, $\Delta\Phi_{\mathrm{wake}}$, fuselage wetted area (SWETF), nacelle wetted area (SWETN)

conditions are established, and 4) Sea Level Static (SLS) where the sea level static thrust target is specified. Each design point requires a specification of the flight Mach number, altitude, and deviation from standard atmosphere temperature (which is set to zero for these cases). Thrust requirements are also specified for SLS, TKO, and TOC, the latter two obtained from an assumed lapse profile. In this study, ADP is set at Mach 0.8, 35,000 ft. TOC is also set at the same flight conditions, but involves operating the fan at a higher speed. TKO and SLS are set at sea level, but TKO is defined at Mach 0.25, while SLS is by definition at static conditions. The MDP process then iteratively varies parameters like airflow rate, fuel to air ratio, etc. to produce an engine model that satisfies the thrust targets and other specified requirements at each of the design conditions. The flow path areas also vary as the MDP solver converges to a final sized engine. The BLI surrogate models are embedded within the NPSS engine model. The mapping between thrust-drag and power balance allows for the BLI effects $P_{K_{\mathrm{in}}}$ and $\Delta\Phi_{\mathrm{wake}}$ to be accounted for as an equivalent force benefit, which is tacked on to the gross thrust calculations for the engine. The pressure recovery losses from the BLI surrogates overwrite the default inlet performance curves. As such, the MDP solver now has to account for changing engine performance capabilities, as the magnitude of the BLI effects varies with fan diameter.

After the engine has been sized for an initial set of thrust requirements and BLI corrections, off design analysis generates the engine decks to be used by FLOPS. In addition, WATE++ provides estimates for the engine weight and critical dimensions, which are used by FLOPS to calculate the nacelle drag. FLOPS' internal aerodynamics prediction capability is used to calculate airframe drag (D'). Corrections to the nacelle and fuselage wetted areas are then applied from the $\Delta\Phi_{\mathrm{surf}}$ surrogates to modify FLOPS estimations for nacelle and fuselage drag. FLOPS sizes the airframe for the specified wing loading, thrust to weight ratio, mission, range constraint, and other airframe design parameters. Based on the gross weight converged on by FLOPS and the user specified wing loading, the wing is resized from the initial guess. This new value is passed back to the surrogates in the subsequent iteration. In addition, the engines are rescaled if they produce more thrust than required for the mission, or are unable to meet the thrust requirements. This scaling factor is applied to the thrust requirements at the engine design points for the next sizing iteration. The sizing

iteration converges when this scale factor equals 1 ± 0.01. Note that Eq. (1) is satisfied at each engine sizing point. The other stopping condition for the vehicle sizing is met when the change in wing area between iterations is less than $5ft^2$.

While the BLI effects surrogates are a function of angle of attack (α), this variable is not recognized by any of the disciplinary analysis codes in EDS. One way of accounting for operating angle of attack in the mission, for the BLI surrogates, is to specify an altitude/angle of attack schedule. Within the range of 0°-4°, higher aircraft angles of attack are likely to be found at low altitudes during takeoff and climb. As the aircraft approaches cruising altitude, the angle of attack is expected to decrease. As such, a step function approach is adopted where for any operating point below 10,000 ft., α is assumed to be 4°. Between 10,000 and 30,000 ft. α is assumed to be 2° and for higher altitudes where the aircraft will cruise, α is set to 0°. Given the sensitivity of the BLI effects to angle of attack, discussed in [38], changes to this schedule will impact the fuel burn estimate of the BLI vehicle. An α sensitivity study is described in the next section that investigates how the assumed angle of attack variations impact the aero-propulsive coupling due to BLI.

The only inputs to the BLI effects surrogates that change in the sizing process are d_2, and S. The fan diameter changes within both process 1 (as part of engine on-design) and as part of process 0 (when the engines are scaled based on airframe performance). The planform area only changes in the outer MDA loop (process 0). For the *coupled BLI sizing, both d_2, and S inputs to the surrogate models are updated with each iteration.*

B. Decoupled BLI Aircraft Sizing

The decoupled approach shown in Fig. 4b is intended to be reflective of the decoupled methods described in literature for BLI modeling. In particular, the system level study for the BWB by Hardin [49] and the STARC-ABL vehicle design study by Welstead [5] are prime examples of this decoupled approach. Both these studies relied on an handful of CFD solutions for the boundary layer, from a fixed aircraft geometry, thereby ignoring the aero-propulsive coupling. To mimic these approaches with the BLI surrogate models, the disciplinary coupling variable inputs to the surrogates, fan diameter and wing planform area, are fixed at their initial guessed values. These quantities are not updated over the course of the sizing loop. The operating condition inputs are allowed to vary for the surrogates, since the decoupled approaches in literature did account for these conditions in some manner. *It should be emphasized that the decoupled approach here solely refers to the treatment of the BLI effects on the aircraft design, and not the entire sizing process.* The engine size is still scaled with the aircraft in an iterative manner as before. It is just that the BLI effects are not corrected for the changing aircraft size. Like in the coupled approach, the decoupled sizing process converges when the thrust scale factor equals 1 ± 0.01. The wing planform area convergence criterion, however, no longer applies. Depending on how good the initial guesses are, there may be a significant discrepancy between the assumed values for fan diameter and planform area used in the BLI surrogates, and the final values from the sized aircraft. In contrast, the coupled approach ensures consistency in these variables.

The differences in aircraft design and performance between the decoupled and coupled approaches depend on the

initial guess provided for fan diameter and wing planform area. A poor guess will result in a mis-estimation of the BLI effects. A reduction in wetted area, engine pylon weight, along with $P_{K_{\text{in}}}$ and $\Delta\Phi_{\text{wake}}$ reduce engine thrust requirements, allowing for a smaller engine. However, boundary layer blockage effects need to be accounted for, and the drop in engine performance due to a loss in pressure recovery both tend to result in a larger fan diameter. The larger engine is heavier, has more wetted area, which tends to increase the thrust requirements, counteracting some of the aforementioned benefits. While a larger fan implies more BLI, this is not necessarily optimal for performance. Additionally, changes in fuel and engine weight also affect the wing size, which in turn has a direct impact on both aircraft drag and the BLI effects. Given all these competing interactions, picking a suitable initial guess can be challenging. A justifiable initial guess for fan diameter and wing planform area could be one obtained from an equivalent non-BLI baseline. This strategy would be consistent with the decoupled approaches in literature, where the CFD profiles were obtained from a representative non-BLI aircraft. If BLI related aero-propulsive coupling is weak, then design and performance differences between the decoupled and coupled approaches will be small and the initial guesses do not matter as much. If the coupling is stronger, more significant differences are expected, justifying the need for the methodology proposed in this paper.

VI. Initial Design Space Exploration with Aero-Propulsive Coupling

In early conceptual design, fan pressure ratio (FPR) represents a major engine cycle parameter that designers vary to optimize propulsive efficiency. A decrease in FPR results in an increase in fan diameter and thus higher propulsive efficiency for the same requirements. However, weight and aerodynamic drag penalties from lower FPR engines tend to offset some of the propulsive efficiency benefits. On the airframe side, wing loading (WSR) is one of the primary variables that controls the wing size for a given gross weight. Wing loading is driven by takeoff and landing performance, as well as maneuverability, but, the wing size also has an impact on overall vehicle drag and weight. Reducing wing loading increases the wing planform area. As discussed previously, wing size and fan diameter are key variables that vary as part of the aircraft sizing process and also have an impact on the BLI effects. As such, FPR and WSR are ideal initial candidates for a parameter sweep to investigate how aero-propulsive coupling due to BLI has an impact on fuel burn predictions in early conceptual design.

A. Fan Pressure Ratio and Wing Loading Sweep

In the following experiments, first, design fan pressure ratio is varied between 1.48 and 1.60 for a constant value of wing loading at 131.4 lbf/ft^2, for the non-BLI and BLI versions of both aircraft configurations shown in Fig. 2. Then, wing loading is varied between 115 to 145 at a fixed FPR of 1.54. The non-BLI variants for each case are analyzed first. These non-BLI aircraft exist only as FLOPS and NPSS models of airframe and engine respectively, without any CFD input. The non-BLI aircraft sizing process is similar to that described in Sec. V, without the BLI performance impacts. The idea here is to take these non-BLI aircraft as starting points, and then morph them into the final BLI vehicles by

accounting for the BLI effects, the aero-propulsive coupling, and the resulting changes to the airframe and engine design as a result of BLI. The key enablers in this process are the surrogate models of the BLI effects.

Each aircraft configuration in these experiments is sized for a design range requirement of 3450 n.mi., making the fuel weight and gross weight a fallout of the aircraft sizing process. The design payload is 180 passengers plus baggage. The mission involves takeoff and landing at standard sea level conditions, with a step cruise at Mach 0.78 from 35,000 ft. to 39,000 ft. The FLOPS models are set up for a minimum fuel to climb profile, with descent at the optimal lift to drag ratio. The initial engine for all cases in this parameter sweep is the baseline model shown in Fig. 2, noting that the final sized engine for each case changes due to the BLI effects and variations in FPR and WSR. The mechanical design characteristics of the engines and architecture, however, are fixed. With respect to the shared design variables, $\mathbf{x}_S$, listed in Table 3, the wing aspect ratio is set to 9.2, the leading edge sweep is set at 28°, the taper ratio is 0.3, and the fuselage ramp angle (for the BLI aircraft) is set to 16°.

The sized fan diameter (d_2) and wing planform area (S) for each non-BLI case are used as inputs for the decoupled-BLI runs. The metric of interest, design block fuel, accounts for fuel burn during the design mission and during taxi in. Fig. 5 shows the block fuel requirements for the top-engine configuration for the non-BLI, BLI-decoupled, and BLI-coupled variants, while Fig. 6 shows the same for the side-engine configuration. In all cases, fuel burn savings going from the non-BLI to the BLI variant is observed, as expected. With regards to FPR, both the BLI and non-BLI variants exhibit similar trends. Typically, for a large variation in FPR, a fuel burn bucket is observed, where the fuel burn is minimized at some FPR value. Moving away from that point in either direction results in an increase in fuel burn. The aerodynamic and weight penalties of large nacelles for low FPR engines outweigh the propulsive efficiency benefits, resulting in an increase in fuel burn with a decrease in FPR. This trend is observed in both Fig. 5 and Fig. 6. The BLI vehicle fuel burn increase with a decrease in FPR is much flatter for lower FPR values, compared to the non-BLI vehicle. This behavior is explained by the BLI benefit from larger fans offsetting the aerodynamic penalty to a certain extent, which is

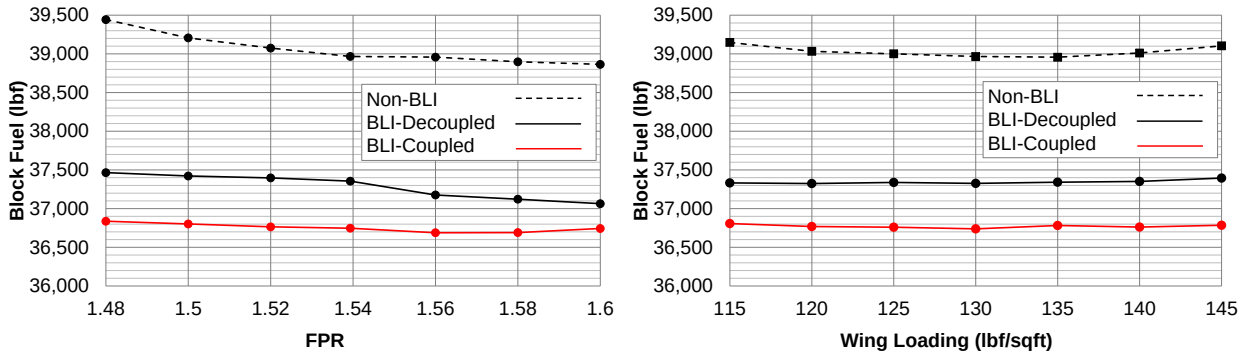

(a) FPR sweep for WSR=131 lbf/ft^2

(b) WSR sweep for FPR = 1.54

Fig. 5 Significant differences in block fuel requirements for the top engine configurations, comparing decoupled to coupled (adapted from [41])

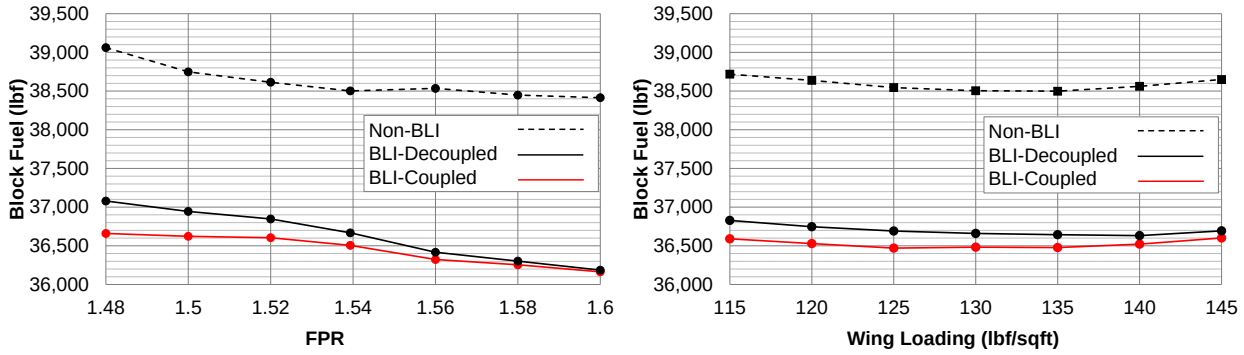

(a) FPR sweep for WSR=131 lbf/ft^2

(b) WSR sweep for FPR = 1.54

Fig. 6 Smaller differences in block fuel requirements between coupled and decoupled, for the side engine configurations (adapted from [41])

obviously not a factor for the non-BLI variant. On the other end, the lower propulsive efficiency of high FPR engines eventually outweighs the aerodynamic and weight benefits of smaller engines, resulting in an increase in block fuel with an increase in FPR. This behavior is not observed in the results because the upper bound of FPR considered, based on the fan diameter constraint, is not high enough for the propulsive efficiency penalties to dominate. Fuel burn trends with wing loading are again similar for both BLI and non-BLI variants and exhibit a slight bucket as expected. The increase in fuel burn on either side of the optimum is due to an increase in vehicle drag, but due to different mechanisms. The drag increase is primarily driven by parasitic drag as the wing wetted area increases for a lower wing loading. On the other hand, the smaller wing area from a higher wing loading results in induced drag penalties.

Now, with regards to the differences between the coupled and decoupled methods, there are two main takeaways from Fig. 5 and 6:

1) There are significant discrepancies in the block fuel burn estimates for a fixed range constraint
2) These differences are more pronounced for the top-mounted engine, given the wing influence on the ingested inflow, as shown in [38]

The decoupled approach consistently over-predicts the block fuel requirements for these cases, compared to the coupled method. The initial guesses for d_2 and S result in an under-estimation of pressure recovery, as well as the propulsive power benefit from $P_{K_{\text{in}}}$ and $\Delta\Phi_{\text{wake}}$, since all three metrics show a strong positive correlation with fan diameter [39]. As a consequence, the converged d_2 and S for the decoupled BLI aircraft are larger than those predicted by the coupled approach, as seen in Fig. 7 for the top-engine configuration. Conversely, if the d_2 and S inputs to the BLI surrogates for the decoupled approach were higher than the converged results from the coupled approach, the BLI benefit would be over-predicted. Consequently, the final converged values of d_2 and S for the decoupled approach would be lower than the coupled results. The discrepancy between the decoupled and coupled approaches is the smallest when either the initial d_2 and S inputs for the BLI surrogates are close to the converged coupled values, or, when the BLI related

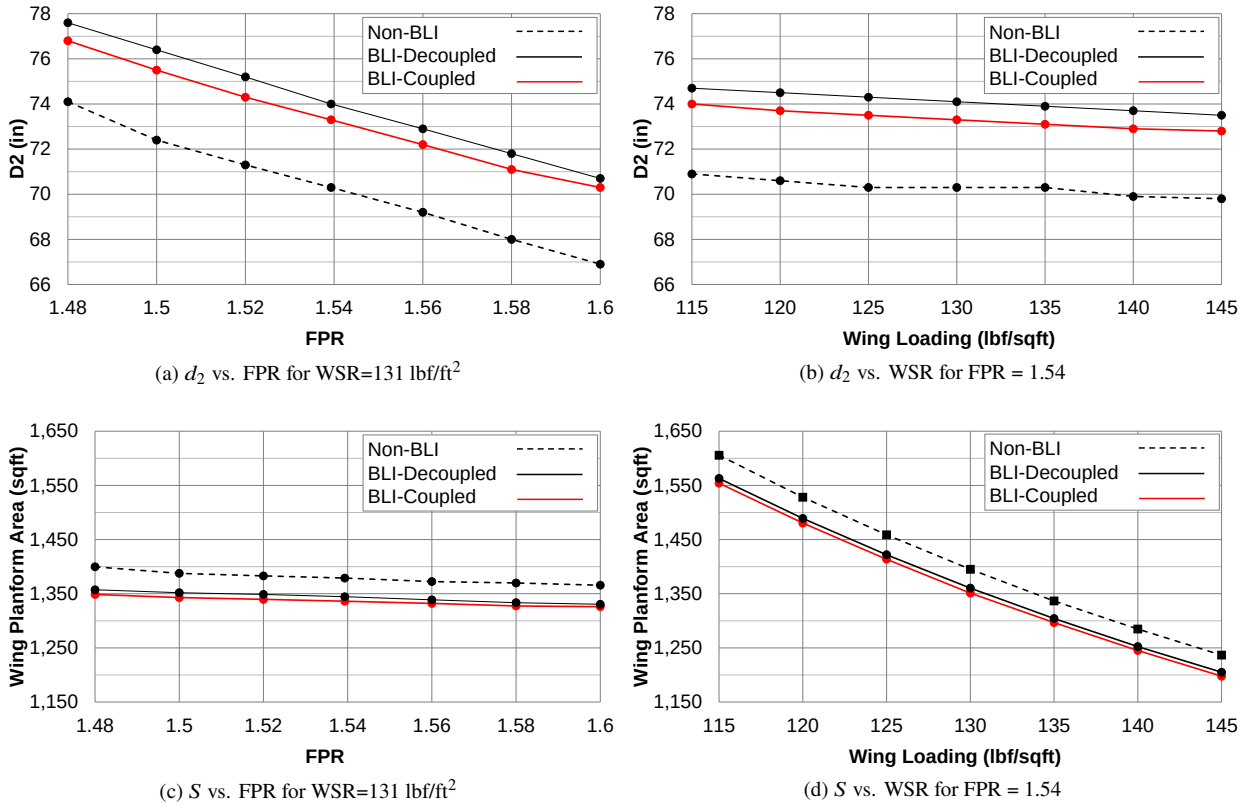

(a) d_2 vs. FPR for WSR=131 lbf/ft^2

(b) d_2 vs. WSR for FPR = 1.54

(c) S vs. FPR for WSR=131 lbf/ft^2

(d) S vs. WSR for FPR = 1.54

Fig. 7 Variations in d_2 and S vs. FPR and WSR for the top engine configurations (adapted from [41])

aero-propulsive coupling is weaker, as evident in the side engine block fuel results in Fig. 6, and the comparison of the final d_2 and S values for the aircraft in Fig. 8.

The results in Fig. 8 suggest that while BLI does have an impact on the sized vehicle, based on the difference between the BLI and non-BLI curves, the aero-propulsive coupling due to BLI is a lot weaker than observed for the top-engine configuration. As a result, even though the non-BLI values of d_2 and S, which are used as inputs for the decoupled approach BLI surrogates, are considerably different from the converged BLI results, variations in d_2 and S as part of the sizing process have a smaller impact on the BLI effects for this engine location. Thus, the coupled approach results are not much different from the decoupled approach. Another interesting observation is that the discrepancy between the coupled and decoupled approaches reduces with an increase in FPR and WSR (a decrease in d_2 and S). For larger fans, there is more BLI. Thus, the d_2 and S inputs based off the non-BLI configuration, are further away from the 'true' converged solutions from the coupled approach. For smaller fans with less BLI, relative variations in the BLI effects due to aero-propulsive coupling are less significant when compared to the net BLI effect over a non-BLI vehicle. Thus, while the MDA process is still able to converge to a BLI configuration with a relatively consistent difference in d_2, S, and block fuel, to the equivalent non-BLI configuration, the differences between the coupled and decoupled approaches decreases.

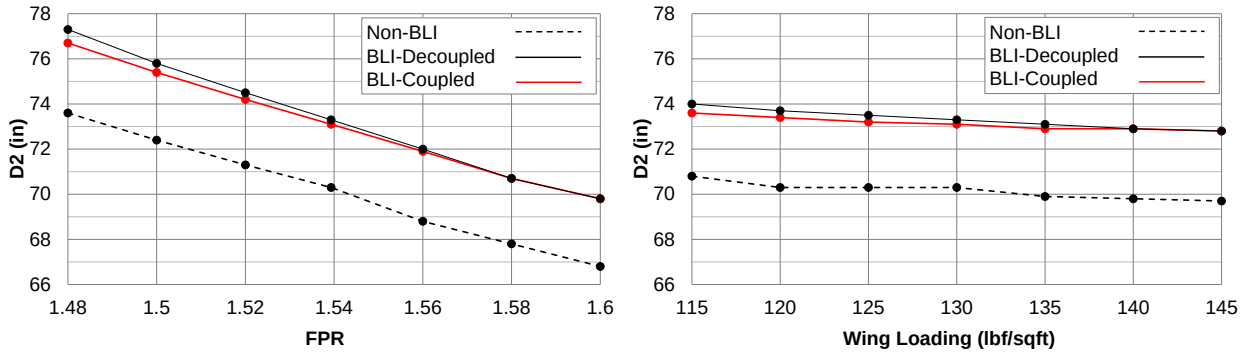

(a) d_2 vs. FPR for WSR=131 lbf/ft^2 (b) d_2 vs. WSR for FPR = 1.54

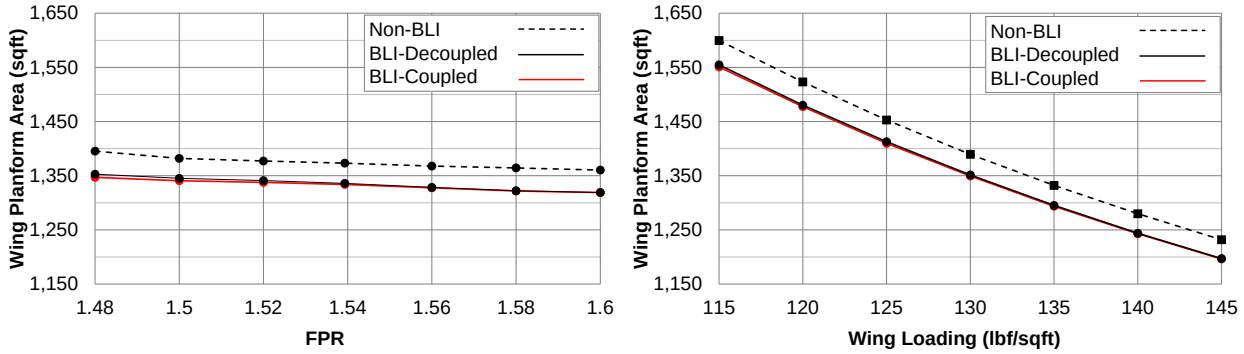

(c) S vs. FPR for WSR=131 lbf/ft^2 (d) S vs. WSR for FPR = 1.54

Fig. 8 Variations in d_2 and S vs. FPR and WSR for the side engine configurations (adapted from [41])

Fig. 9 shows the percentage difference in the block fuel burn estimate between the decoupled (D) and coupled (C) approaches ($100 \times \frac{D-C}{C}$), comparing it between the top and side engine configurations for each case in the FPR and WSR sweeps. The trends observed support the above discussion. The largest difference in the predicted fuel burn between the decoupled and coupled approaches is about 1.7% (628 lbf) for the top-engine configuration at FPR=1.48

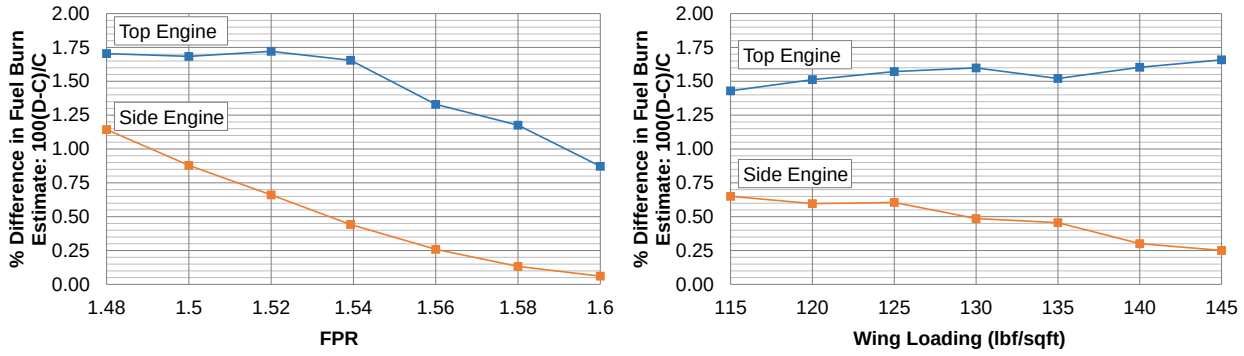

(a) FPR sweep for WSR=131 lbf/ft^2 (b) WSR sweep for FPR = 1.54

Fig. 9 Percentage difference in the block fuel burn estimates (coupled vs decoupled) for the top engine configurations are larger than those for the side engine configuration (adapted from [41])

for WSR=131.4lbf/ft^2. The fuel burn reduction benefit, comparing the coupled result to the same non-BLI design point is 6.6% (2606 lbf). Thus, the fuel burn discrepancy based on using a decoupled approach instead of a coupled, as a percentage of the fuel burn savings going from non-BLI to BLI ($100 \times \frac{D-C}{\text{No-BLI}-C}$), is about 24% for this design. This difference is a substantial portion of the predicted BLI-benefit. While it is difficult to comment on how discrepancies between decoupled and coupled approaches seen for these configurations would translate to other kinds of BLI aircraft, like the STARC-ABL for example, the current results clearly highlight how not modeling the aero-propulsive coupling can be a significant source of uncertainty in the fuel burn savings numbers quoted in literature.

B. A Few Additional Comments on Presented Results

The vehicle sizing process can be thought of a numerical scheme for solving a system of equations that results in an appropriately sized engine and airframe that meet the specified requirements. As such, both the initial estimates needed to solve the system and the convergence criteria play a role in affecting the outcome. There are multiple 'solver loops' involved in the vehicle sizing process. The engine multi-design point sizing approach, in particular, is a critical component. The convergence success of this method was found to be sensitive to the initial required thrust estimates specified at different design points, more so for the BLI cases than for the non-BLI ones. Since both used the same initial guesses, derived from the non-BLI cases, this is not unexpected. In essence, the Broyden solver coded in NPSS is attempting to design an engine that satisfies Eq. (1) at each of the specified design points. As the solver varies the required flow rate and fan diameter, among other variables, to match the specified thrust targets, the impact of the BLI effects on engine performance also change. This coupling between engine design and operation, and the BLI effects, makes convergence for BLI engine design more challenging than for the non-BLI case. Some cases diverged in the engine sizing phase. However, those that did converge were found to be insensitive to the initial guesses, as expected. The failed cases were re-run after applying small perturbations to the initial thrust targets, on the order of 100 pounds or less, through a trial and error approach.

The solutions of the entire vehicle sizing process, i.e., the outer MDA loop (process 0 in Fig. 4), are to a certain extent dependent on the the tolerances specified for the convergence criteria, primarily on the engine scale factor. The tolerance of 0.01 on the engine scale factor condition allows for a small margin of variation in the sized engine thrust, relative to the specified thrust to weight requirement. As such, relative to the perfect scenario where the scale factor is exactly 1, there are slight discrepancies in engine size, weight, and thus overall gross weight and fuel burn. In other words, the range of permissible engine scale factors from 0.99 to 1.01 introduces a certain degree of noise into the results. While several cases fall within a much narrower band around 1, some however did reach the limits set by the tolerance. In the end, the magnitude of this noise was deemed acceptable for the purposes of this study, after noting that the main conclusions are not affected by the noise. Additionally, decreasing the tolerance would have increased the number of iterations required for convergence.

Now, a few comments need to be made with regards to the BLI fuel burn benefit observed relative to the non-BLI configuration. For the top-engine vehicle in the FPR sweep, there is a fuel burn reduction for the coupled-BLI configuration in the range of 5.5% to 6.6%, and for the WSR sweep, between 5.6% to 6% relative to the non-BLI aircraft. For the side-engine configuration, the coupled-BLI fuel burn reduction varies between 5.2% and 6.1% for the FPR sweep and between 5.2% to 5.5% for the WSR sweep. *These differences in fuel burn are solely due to BLI and not due to the addition of technologies on the BLI configuration that are not on the non-BLI variants*. While quantifying the BLI benefit relative to a non-BLI configuration is not the primary purpose of this study, it should be noted that the fuel burn reductions calculated here are still within expectations. Context can be obtained by looking at some system level BLI studies in literature that have quoted fuel burn reduction numbers. Hardin [49] showed a 3-5% BLI fuel burn benefit for the N+2 BWB concept relative to an appropriate BWB baseline with podded engines. This benefit increased to around 10% for the N+3 BWB concept. Yutko [8] showed a 26-27% block fuel reduction for the D8 compared to the 737-800. Welstead [5] showed a 12% reduction in design block fuel burn for the STARC-ABL, compared to a N3CC non-BLI reference with TRL 6 technologies. In context of the above results, the predicted system level fuel burn savings of 5-7%, using current state of the art technologies for both the BLI and non-BLI variants, is not unrealistic.

C. Sensitivity to Angle of Attack Assumptions

To determine whether the assumed angle of attack variation with altitude (h) affects the conclusions drawn above, α is changed and the FPR sweep is rerun for both the top and side-engine aircraft. The following schedules are investigated:

1) Fixed $\alpha = 3^\circ$ over the entire flight envelope
2) Fixed $\alpha = 1^\circ$ over the entire flight envelope
3) Varied $\alpha = 4^\circ$ for $h < 10,000$ft., $\alpha = 3^\circ$ for $10,000 \leq h < 30,000$ft. and $\alpha = 2^\circ$ for $h \geq 30,000$ft.

The following observations can be made from the results presented in Fig. 10, which includes trends from Fig. 9a for reference:

1) Regardless of the angle of attack assumption, differences between coupled and decoupled fuel burn estimates are larger for the top-engine configurations compared to the side engine case
2) In general, the difference between coupled and decoupled fuel burn estimates reduces with FPR
3) The discrepancy between decoupled and coupled estimates tends to worsen with an increase in angle of attack for the top-engine cases, with the opposite observed for the side-engine configurations

Observations 1 and 2 are consistent with the results shown previously and can be explained in a similar manner as before. There are a number of factors that are likely at play with respect to observation 3. Findings from [38] show differences in the boundary layer development over the top and side of the fuselage, and were linked to the combined effects of wing downwash and angle of attack. For the top-engine cases, a higher angle of attack corresponds to a thicker ingested boundary layer. A larger diameter (lower FPR) corresponds to more BLI. As such, the combined effects of the

two suggest that the predictions from the decoupled cases, which only use a fixed value of fan diameter to estimate the BLI effects, are progressively worse as the amount of BLI increases. The trends for the side engine case imply that the sensitivity of the BLI effects to changes in fan diameter is lower as angle of attack increases. The flow development over the side of the fuselage, relative to angle of attack changes, is not as intuitive as it is for the top. As such there are differences in the way the boundary layer flow develops and what portion of the boundary layer and freestream flow is ingested by the propulsor as the diameter changes. In general, it appears that the variations in the BLI effects due to changes in fan diameter are smaller for the side engine cases, which means that the coupled and decoupled results are very similar.

The observations above lend further support to the claim that aero-propulsive interactions due to BLI must be captured as part of the design methodology. While sensitivity of the BLI effects to angle of attack is captured in the surrogates, the results in Fig. 10 motivate the need for a modified mission analysis for BLI applications rather than relying on user assumed h-α schedules like above. The requirement would be to account for and optimize the operating angle of attack of the vehicle throughout the mission, while interacting with the BLI effects surrogates at each step. At this point, angle of attack would become a coupling variable.

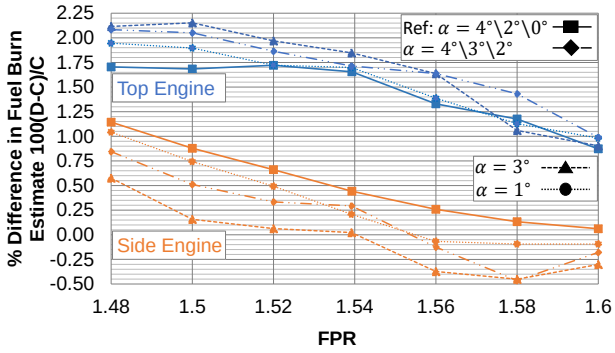

Fig. 10 Fuel burn estimates still show substantial differences between decoupled and coupled approaches for regardless of h-α assumptions (adapted from [41])

VII. Extended Design Space Exploration with Aero-Propulsive Coupling

The fan pressure ratio and wing loading sweep study can be extended to consider additional airframe and cycle design variables to see if previously drawn conclusions still hold. The design variables considered in this short study are shown in Table 4. While sensitivity of the discrepancies between coupled and decoupled results to angle of attack was noted above, development of an angle of attack sensitive mission analysis was out of scope for this present effort. As such, the original h-α schedule is assumed for these experiments.

An overall pressure ratio (OPR) constraint in the range of 45-55 (assuming duct losses) is imposed on the design space based on expected values for a direct drive fan in the 2035 time frame. This constraint filters out infeasible

Table 4 Design Variables for Design Space Exploration

Input Variable	Lower Bound	Upper Bound	Type	Comments
FPR	1.48	1.60	Propulsor	OPR Constraint 45-55
LPCPR	1.25	2.25	Propulsor	OPR Constraint 45-55
HPCPR	15	35	Propulsor	OPR Constraint 45-55
AR	7	11	Airframe	
λ	0.2	0.4	Airframe	
$\Lambda_{c/4}$ (°)	20	40	Airframe	Λ_{LE} constraint 20°-40°
ϕ (°)	12	20	Airframe	
WSR	115	145	Airframe	

combinations of FPR, low pressure compressor pressure ratio (LPCPR), and high pressure compressor pressure ratio (HPCPR) within the specified bounds. A leading edge sweep constraint between 20°-40° is also imposed. FLOPS internal aerodynamics are based on quarter chord sweep ($\Lambda_{c/4}$). The BLI surrogates, however, were modeled using leading edge sweep. Since the mapping between quarter chord and leading edge sweep is based on taper ratio (λ) and aspect ratio (AR), the leading edge sweep constraint filters out disallowed combinations of AR, λ, and $\Lambda_{c/4}$. Two space filling DOEs are created in the JMP program for the BLI studies. Each DOE has 2000 cases that are split 75%-25% for training and validation. There are enough cases within each DOE to account for significant non-linearity in the responses and failed cases due to convergence issues. The metrics of interest are design block fuel, d_2, S, takeoff gross weight (TOGW), and sea level static (SLS) thrust per engine. The responses for each sample point in the DOE are obtained from EDS using the proposed BLI aircraft sizing methodology. An artificial neural network model is used to fit each response and then evaluated against the 'goodness of fit' metrics alluded to in context of the BLI surrogates.

The design space can be viewed through a series of profiler plots generated by JMP. The neural network models behind these trends form a fully parametric environment, where the design point can be easily changed to observe corresponding changes to the system level responses. Fig. 11 compares the decoupled and coupled trends for the top-engine configuration, while Fig. 12 does the same for the side-engine vehicle. Consistent with the previous study, there are noticeable differences between the decoupled and coupled trends for the top-engine configuration, which are much smaller for the side-engine aircraft. There is also agreement between the surrogate model trends for block fuel, d_2, and S with FPR and WSR, and the EDS results presented previously, which verifies that the surrogate models are capturing the correct trends.

To minimize fuel burn, the plots suggest higher pressure ratios and aspect ratio as expected. A lower taper ratio is desirable to maintain an elliptical lift distribution, while interestingly, smaller sweep angles also appear to minimize fuel burn. For a transonic aircraft, increasing sweep decreases drag, but also lowers lift. Depending on the operating weight of the vehicle and the required lift at a given flight condition, increasing sweep may not be optimal. In addition, for a given wing span, increasing sweep increases the length of the wing spars and their required stiffness must also

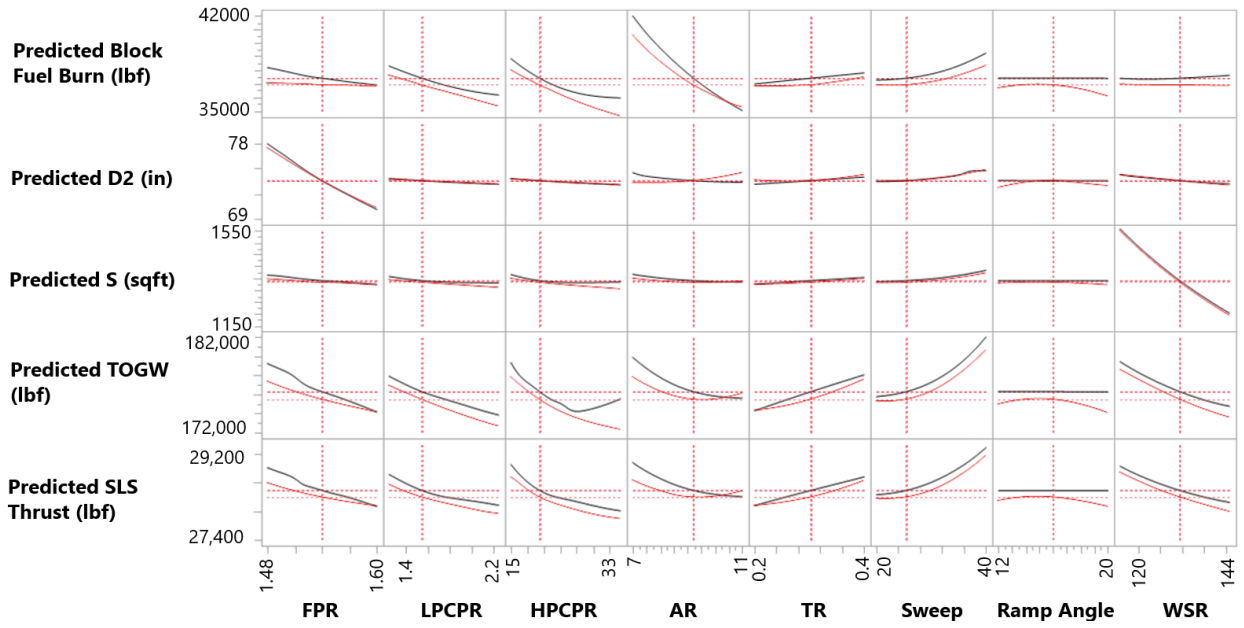

Fig. 11 Top-Engine BLI profiler plots showing trends of key metrics with the design variables. The coupled approach trends are shown in red and the decoupled in black (adapted from [41])

increase. Consequently, wing weight increases with sweep, which has an adverse impact on required block fuel. A bucket shaped variation of the coupled fuel burn profile with ramp angle (ϕ) is due to the competing effects of $P_{K_{\text{in}}}$, $\Delta\Phi_{\text{wake}}$, and pressure recovery. Experiment 8 in [38] showed that both $P_{K_{\text{in}}}$ and $\Delta\Phi_{\text{wake}}$ increased with ramp angle, but pressure recovery decreased. In Fig. 11 for example, $\phi = 12^\circ$ and $\phi = 20^\circ$ show the lowest fuel burn for the selected design point, with the latter appearing to be the global optimum. Increasing block fuel burn with an increase in the ramp angle from 12° suggests that the pressure recovery losses are more dominant, but after a certain value, the $P_{K_{\text{in}}}$ and $\Delta\Phi_{\text{wake}}$ benefits overcome these losses.

TOGW variations are driven by changes in fuel weight and structural weight. As such, discrepancies in design characteristics and fuel burn predictions between the decoupled and coupled approaches can either compound, or offset, when considering gross weight. An example of this effect can be seen in the differences between TOGW decoupled and coupled trends with aspect ratio. The coupled approach correctly predicts the BLI effects and as such, the fuel burn variation with aspect ratio is more gradual compared to the decoupled predictions. Additionally, higher aspect ratio wings are heavier. After a certain point, the structural weight penalty should offset the fuel burn savings and TOGW should increase. While this behavior is captured by the coupled trends, the decoupled fuel burn predictions offset the structural weight increase from higher aspect ratio wings, to a point where a TOGW bucket with AR is not observed in this design space for the decoupled approach. For the other design variables considered in this exercise, it appears that variations in fuel burn primarily affect the TOGW trends. This explains why a reduction in TOGW is achieved by increasing FPR, LPCPR, HPCPR, and decreasing sweep and taper ratio.

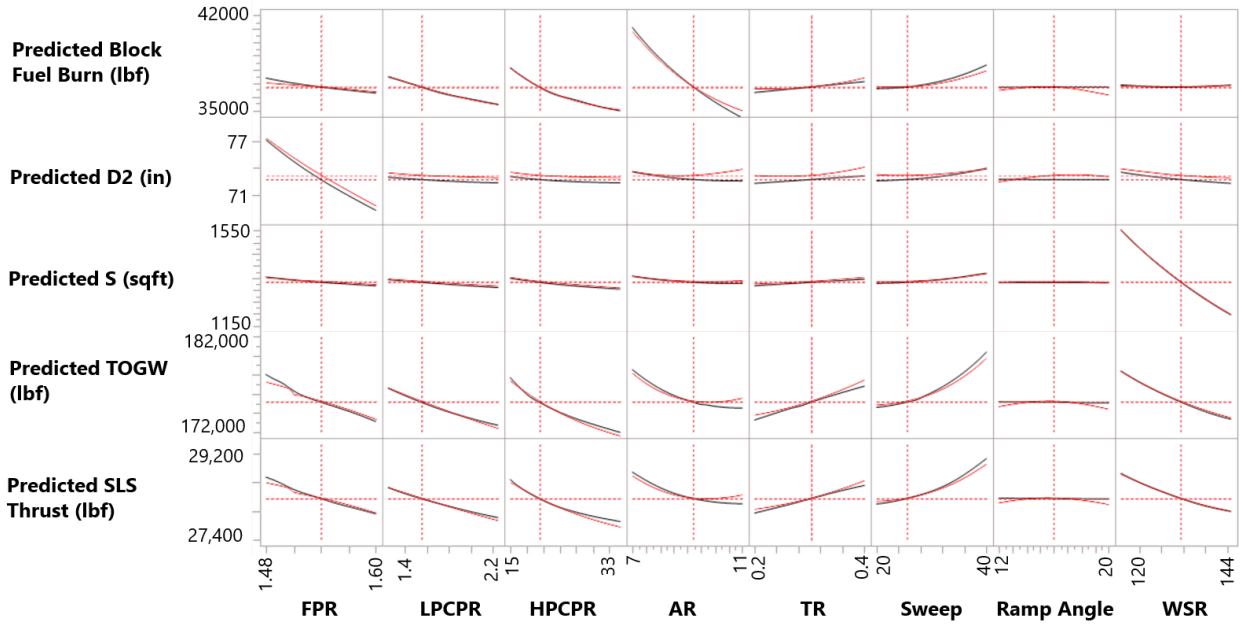

Fig. 12 Side-Engine BLI profiler plots showing trends of key metrics with the design variables. The coupled approach trends are shown in red and the decoupled in black (adapted from [41])

It should be noted that the trends observed in these figures can change depending on the design point picked in the profile, due to interactions between the variables. Also, if angle of attack was considered as a coupling variable in the mission analysis, rather than a static input to the surrogates, then the observed trends could impacted as well. As such, while it is premature to predict what an optimized vehicle would look like from just these trends, one major conclusion can still be seen from the results; aero-propulsive interactions can have a significant effect on the performance predictions for a BLI configuration and therefore should be considered in early conceptual design.

VIII. Concluding Remarks

The results from this study clearly show the scope of potential uncertainty in BLI aircraft design and performance by using a decoupled approach instead of a coupled. As observed in the first set of experiments for example, the discrepancy in fuel burn introduced by using a fixed point design estimate (decoupled approach) for the BLI effects, instead of a parametric and coupled estimation, can be anywhere in the range of 0.06% to 1.7%, depending on the aircraft design, engine location, and assumed angle of attack. As a fraction of the predicted BLI fuel burn savings relative to the non-BLI configuration, this error due to ignoring aero-propulsive coupling can be as high as 24%. A caveat to the results in this paper concerns the role of operational uncertainty. Fig. 10 showed how the fuel burn predictions changed based on the angle of attack assumptions. A consequence of this uncertainty is the discrepancy between the decoupled and coupled fuel burn predictions, which went as high as 2.15%. The sensitivity of aero-propulsive coupling to angle of attack motivates the need for a modified mission analysis for BLI concepts. Here, not only should the sensitivity of the

BLI effects to angle of attack be accounted for, like in this study, but also, the sensitivity of fuel burn to operational angle of attack and the ability to optimize the geometry and/or operation in conjunction with the BLI effects surrogate models to minimize fuel burn must be possible. In short, there is a need to promote angle of attack as a coupling variable, rather than treating it as a static assumption.

There are also a few drawbacks with the proposed conceptual design method. The prohibitive cost of directly linking CFD with mission analysis and engine cycle design necessitates surrogate modeling techniques. Thus, the BLI effects are subject to a certain degree of uncertainty with respect to model prediction error, which unfortunately is inherent with any surrogate based approach. Additionally, surrogate models suffer from the the curse of dimensionality, where the number of samples required to generate an accurate surrogate exponentially increases with the number of design variables. As such, when generating surrogates of the BLI effects, the design space needs to be relatively small. If additional design variables are to be considered when formulating surrogates of the BLI effects, dimensionality reduction techniques need to be considered to keep the surrogate model development cost low.

Despite these acknowledged sources of uncertainty and drawbacks that arise from pragmatic implementation methods, the trends show strong support for use of coupled and parametric methodologies for BLI concept design. The conclusions drawn in this study are based on differences in performance and design between coupled and decoupled approaches. These conclusions should be valid regardless of the implementation methods, since the same modeling technique is used for all experiments. The proposed method thus serves as a foundation for future BLI concept design studies.

References

[1] Suder, K., "Overview of the NASA Environmentally Responsible Aviation Project's Propulsion Technology Portfolio," *48th AIAA/ASME/SAE/ASEE Joint Propulsion Conference & Exhibit, Joint Propulsion Conferences*, AIAA, 2012. https://doi.org/10.2514/6.2012-4038.

[2] Muller, R., "ACARE Goals (AGAPE) Progress Evaluation, Project Final Report Publishable Summary," Report, Advisory Council for Aeronautics Research in Europe, 2010.

[3] Betz, A., *Introduction to the Theory of Flow Mechanics*, 1st ed., Pergamon Press, Karlsruhe, Germany, 1966.

[4] Secchi, M., Teixeira, P. L., Trapp, L. G., and Ribeiro, R. F. G., "Evaluation of a Regional Aircraft with Boundary Layer Ingestion and Electric-Fan Propulsor," *Journal of Aircraft*, 2021. https://doi.org/10.2514/1.C035932.

[5] Welstead, J. R., and Felder, J. L., "Conceptual Design of a Single-Aisle Turboelectric Commercial Transport with Fuselage Boundary Layer Ingestion," *AIAA SciTech Forum*, AIAA, 2016. https://doi.org/10.2514/6.2016-1027.

[6] Greitzer, E. M., Bonnefoy, P. A., De la Rosa Blanco, E., Dorbian, C., Drela, M., and Hall, D. K., "N+3 Aircraft Concept Designs and Trade Studies, Final Report," Report, NASA Glenn Research Centre, 2010.

[7] Drela, M., "Development of the D8 Transport Configuration," *AIAA Applied Aerodynamics Conference*, AIAA, 2011. https://doi.org/10.2514/6.2011-397.

[8] Yutko, B., Titchener, N. A., Courtin, C., Lieu, M. K., Wirsing, L., Tylko, J., Chambers, J., Roberts, T., and Clint, C., "Conceptual Design of a D8 Commercial Aircraft," *AIAA Aviation Forum*, AIAA, 2017. https://doi.org/10.2514/6.2017-359.

[9] Wiart, L., Atinault, O., Grenon, R., Paluch, B., and Hue, D., "Development of NOVA Aircraft Configurations for Large Engine Integration Studies," *33rd AIAA Applied Aerodynamics Conference*, AIAA, 2015. https://doi.org/10.2514/6.2015-2254.

[10] Blumenthal, B. T., Elmiligui, A. A., Geiselhart, K. A., Campbell, R. L., Maughmer, M. D., and Schmitz, S., "Computational Investigation of a Boundary-Layer-Ingestion Propulsion System," *Journal of Aircraft*, Vol. 55, No. 3, 2018. https://doi.org/10.2514/1.C034454.

[11] Felder, J. L., Kim, H. D., and Brown, G. V., "Turboelectric Distributed Propulsion Engine Cycle Analysis for Hybrid-Wing-Body Aircraft," *47th AIAA Aerospace Sciences Meeting including the New Horizons Forum and Aerospace Exposition*, AIAA, 2009. https://doi.org/10.2514/6.2009-1132.

[12] Felder, J. L., Kim, H. D., Brown, G. V., and Chu, J., "An Examination of the Effect of Boundary Layer Ingestion on Turboelectric Distributed Propulsion Systems," *49th AIAA Aerospace Sciences Meeting including the New Horizons Forum and Aerospace Exposition*, AIAA, 2011. https://doi.org/10.2514/6.2011-300.

[13] Rodriguez, D. L., "Multidisciplinary Optimization Method for Designing Boundary-Layer-Ingesting Inlets," *Journal of Aircraft*, Vol. 46, No. 3, 2009. https://doi.org/10.2514/1.38755.

[14] Gray, J. S., Mader, C. A., Kenway, G. K., and Martins, J. R. R. A., "Modeling Boundary Layer Ingestion Using a Coupled Aeropropulsive Analysis," *Journal of Aircraft*, Vol. 55, No. 3, 2018. https://doi.org/10.2514/1.C034601.

[15] Gray, J. S., Kenway, G. K., Mader, C. A., and Martins, J. R. R. A., "Aeropropulsive Design Optimization of a Turboelectric Boundary Layer Ingestion Propulsion System," *Aviation 2018*, AIAA, 2018. https://doi.org/10.2514/6.2018-3976.

[16] Gray, J. S., and Martins, J. R. R. A., "Coupled Aeropropulsive Design Optimization of a Boundary Layer Ingestion Propulsor," *The Aeronautical Journal*, Vol. 123, No. 1259, 2018, p. 19. https://doi.org/10.1017/aer.2018.120.

[17] Gray, J. S., Mader, C. A., Kenway, G. K. W., and Martins, J. R. R. A., "Coupled Aeropropulsive Optimization of a Three-Dimensional Boundary-Layer Ingestion Propulsor Considering Inlet Distortion," *Journal of Aircraft*, Vol. 57, No. 6, 2020. https://doi.org/10.2514/1.C035845.

[18] Kim, H., and Liou, M.-S., "Optimal Shape Design of Mail-Slot Nacelle on N3–X Hybrid Wing-Body Configuration," *31st AIAA Applied Aerodynamics Conference*, AIAA, 2013. https://doi.org/10.2514/6.2013-2413.

[19] Kim, H., and Liou, M.-S., "Optimal Inlet Shape Design of N2B Hybrid Wing Body Configuration," *48th AIAA/ASME/SAE/ASEE Joint Propulsion Conference & Exhibit*, AIAA, 2012. https://doi.org/10.2514/6.2012-3917.

[20] Bijewitz, J., Seitz, A., Hornung, M., and Isikveren, A. T., "Progress in Optimizing the Propulsive Fuselage Aircraft Concept," *Journal of Aircraft*, Vol. 54, No. 5, 2017. https://doi.org/10.2514/1.C034002.

[21] Liebeck, R. H., Page, M. A., and Rawdon, B. K., "Blended-Wing-Body Subsonic Commercial Transport," *36th AIAA Aerospace Sciences Meeting and Exhibit*, AIAA, 1998. https://doi.org/10.2514/6.1998-438.

[22] Liebeck, R. H., "Blended Wing Body Design Challenges," *AIAA International Air and Space Symposium and Exposition: The Next 100 Years*, AIAA, 2003. https://doi.org/10.2514/6.2003-2659.

[23] Liebeck, R. H., "Design of the Blended Wing Body Subsonic Transport," *Journal of Aircraft*, Vol. 41, No. 1, 2004. https://doi.org/10.2514/1.9084.

[24] Hileman, J., Spakovszky, Z., Drela, M., and Sargeant, M. A., "Aerodynamic and Aeroacoustic Three-Dimensional Design for a "Silent" Aircraft," *44th AIAA Aerospace Sciences Meeting and Exhibit*, AIAA, 2006. https://doi.org/10.2514/6.2006-241.

[25] Hileman, J. I., Spakovszky, Z. S., and Drela, M., "Airframe Design for "Silent Aircraft"," *45th AIAA Aerospace Sciences Meeting and Exhibit*, AIAA, 2007. https://doi.org/10.2514/6.2007-453.

[26] Hall, C. A., and Crichton, D., "Engine Design Studies for a Silent Aircraft," *Journal of Turbomachinery*, Vol. 129, No. 3, 2006, p. 9. https://doi.org/10.1115/1.2472398.

[27] Plas, A. P., Sargeant, M. A., Madani, V., Crichton, D., and Greitzer, E. M., "Performance of a Boundary Layer Ingesting (BLI) Propulsion System," *45th AIAA Aerospace Sciences Meeting and Exhibit*, AIAA, 2007. https://doi.org/10.2514/6.2007-450.

[28] Seitz, A., Bijewitz, J., Kaiser, S., and Wortmann, G., "Conceptual Investigation of a Propulsive Fuselage Aircraft Layout," *Aircraft Engineering and Aerospace Technology*, Vol. 86, No. 6, 2014. https://doi.org/10.1108/AEAT-06-2014-0079.

[29] Hendricks, E., "A Review of Boundary Layer Ingesting Modeling Approaches for use in Conceptual Design," Report, NASA Glenn Research Center, 2018.

[30] Kirby, R., Michelle, and Mavris, D. N., "The Environmental Design Space," *28th International Congress of the Aeronautical Sciences*, ICAS, 2008.

[31] Nunez, L. S., Tai, J., and Mavris, D. N., "The Environmental Design Space: Modeling and Performance Updates," *AIAA SciTech Forum*, AIAA, 2021. https://doi.org/10.2514/6.2021-1422.

[32] McCullers, L. A., "Aircraft Configuration Optimization Including Optimized Flight Profiles," *NASA Symposium on Recent Experiences in Multidisciplinary Analysis and Optimization*, NASA, 1984.

[33] Lytle, J. K., "The Numerical Propulsion System Simulation: A Multidisciplinary Design System for Aerospace Vehicles," *14th International Symposium on Air Breathing Engines*, NASA, 1999.

[34] Tong, M. T., and Naylor, B. A., "An Object-Oriented Computer Code for Aircraft Engine Weight Estimation," *Proceedings of ASME Turbo Expo 2008: Power for Land, Sea and Air*, ASME, 2008. https://doi.org/10.1115/GT2008-50062.

[35] Drela, M., "Power Balance in Aerodynamic Flows," *AIAA Journal*, Vol. 47, No. 7, 2009. https://doi.org/10.2514/1.42409.

[36] Hall, D. K., Huang, A. C., Uranga, A., Greitzer, E. M., Drela, M., and Sato, S., "Boundary Layer Ingestion Propulsion Benefit for Transport Aircraft," *Journal of Propulsion and Power*, Vol. 33, No. 5, 2017. https://doi.org/10.2514/1.B36321.

[37] Hall, D. K., Lieu, M. K., and Drela, M., "Aerodynamic Performance Accounting for Ultra-Integrated Air Vehicle Configurations," *AIAA SciTech Forum*, AIAA, 2019. https://doi.org/10.2514/6.2019-1310.

[38] Ahuja, J., and Mavris, D. N., "Sensitivity of Boundary Layer Ingestion Effects to Tube and Wing Airframe Design Features," *AIAA SciTech Forum*, AIAA, 2020. https://doi.org/10.2514/6.2020-1523.

[39] Ahuja, J., and Mavris, D. N., "Assessment of Propulsor On-Design and Off-Design Impacts on BLI Effects," *AIAA SciTech Forum*, AIAA, 2021. https://doi.org/10.2514/6.2021-0605.

[40] Myers, R. H., Montgomery, D. C., and Anderson-Cook, C. M., *Response Surface Methodology: Process and Product Optimization Using Designed Experiments*, Wiley Series in Probability and Statistics, John Wiley and Sons, Hoboken, NJ, 2009.

[41] Ahuja, J., "A Methodology for Capturing the Aero-Propulsive Coupling Characteristics of Boundary Layer Ingesting Aircraft in Conceptual Design," Thesis, 2020.

[42] McDonald, R. A., and Gloudemans, J. R., "Open Vehicle Sketch Pad: An Open Source Parametric Geometry and Analysis Tool for Conceptual Aircraft Design," *AIAA SciTech Forum*, AIAA, 2022. https://doi.org/10.2514/6.2022-0004.

[43] Vassberg, J., Dehaan, M., Rivers, M., and Wahls, R., "Retrospective on the Common Research Model for Computational Fluid Dynamics Validation Studies," *Journal of Aircraft*, Vol. 55, No. 4, 2018. https://doi.org/10.2514/1.C034906.

[44] EASA, "ICAO Aircraft Engine Emissions Databank," , 2021. URL https://www.easa.europa.eu/domains/environment/icao-aircraft-engine-emissions-databank.

[45] *CFM International LEAP-1B Series Engines Type-Certificate Data Sheet*, Dec. 2019. URL https://www.easa.europa.eu/domains/environment/icao-aircraft-engine-emissions-databank.

[46] Ordaz, I., Rallabhandi, S., Nielsen, E. J., and Diskin, B., "Mitigation of Engine Inlet Distortion through Adjoint-Based Design," *AIAA Aviation Forum*, AIAA, 2017. https://doi.org/10.2514/6.2017-3410.

[47] Schutte, J., "Simultaneous Multi-Design Point Approach to Gas Turbine On-Design Cycle Analysis for Aircraft Engines," Thesis, 2009.

[48] Schutte, J., Tai, J., Sands, J. S., and Mavris, D. N., "Cycle Design Exploration Using Multi-Design Point Approach," *ASME Turbo Expo 2012: Turbine Technical Conference and Exposition*, ASME, 2012. https://doi.org/10.1115/GT2012-69334.

[49] Hardin, L. W., Tillman, G., Sharma, O. P., Berton, J., and Arend, D. J., "Aircraft System Study of Boundary Layer Ingesting Propulsion," *48th AIAA/ASME/SAE/ASEE Joint Propulsion Conference & Exhibit*, AIAA, 2012. https://doi.org/10.2514/6.2012-3993.